A nanoprobe for ratiometric imaging of glutathione in living cells based on the use of a nanocomposite prepared from dual-emission carbon dots and manganese dioxide nanosheets

Zhiwei Deng [1] · Xiufang Li [1] · Hui Liu [1] · Yao He [1] · Jie Zhang [1] · Jing Yuan [1] · Peiru Gao [1] · Xuling Jiang [1] · Yanjing Yang [1] · Shian Zhong [1]

Abstract

A ratiometric fluorescence assay for glutathione (GSH) was developed. The novel assay is based on a nanoprobe composed of manganese dioxide nanosheets (MnO_2 NS) and dual-emission carbon dots (de-CDs) with intrinsic GSH-response property. After construction of the nanoprobe, two emission peaks of de-CDs were suppressed to varying degrees by MnO_2 NS. The suppression was relieved and the two emission peaks recovered proportionally when MnO_2 NS was decomposed by GSH, thus realizing the ratiometric assay for micromolar GSH. The intrinsic responsiveness of de-CDs to millimolar GSH broadens the analytical range of the nanoprobe. An appropriate precursor, calcon-carboxylic acid, was screened out to synthesize de-CDs via one-step hydrothermal treatment. The de-CD@MnO_2 NS nanoprobe can measure GSH concentrations through the fluorescence intensity ratio between 435 and 516 nm excited at 365 nm. The range of response was from 1 μM to 10 mM and the detection limit reached 0.6 μM (3σ criterion). Benefiting from its good biocompatibility, the proposed nanoprobe has excellent applicability for intracellular GSH imaging.

Introduction

Glutathione (GSH) is a major nonprotein thiol which plays important roles in various biological functions, such as the cellular antioxidant defense system, gene regulation, xenobiotic metabolism, and intracellular signal transduction [1–3]. The changes in GSH level are related to many diseases, including leucocyte loss, diabetes, Alzheimer's disease, and Parkinson's [4–6]. Thus, knowledge of the levels of GSH in living cells is crucial for illustrating its accurate cell functions as well as providing pivotal assistance for early diagnosis of diseases. A variety of analytical techniques have been developed for measuring GSH level for biomedical applications [7–12]. Among different kinds of GSH assays, optical methods based on fluorescence techniques have attracted more interest because of the advantages of high sensitivity, spatial resolving power, nondestructiveness, and ease of miniaturization. In particular, ratiometric fluorescence probes, which have the advantages of better selectivity and higher reliability derived from the inherent self-referencing property, are more favorable for assay targets in living cells compared with single-intensity-based probes [13–16]. Accordingly, the development of new fluorescence probes is highly desirable for fluorescence-based ratiometric intracellular GSH assay. However, to the best of our knowledge, the ratiometric GSH-response nanoprobes reported so far are typically based on heavy/noble metal ions that can lead to sample contamination or rely on artificially synthesized organic molecules [17–19]. Engineering of robust and nanomaterial-based ratiometric probes for intracellular GSH imaging is still a big challenge.

✉ Yanjing Yang
  yangyanjing@csu.edu.cn

✉ Shian Zhong
  zhongshian@aliyun.com

[1] College of Chemistry and Chemical Engineering, Central South University, Changsha 410083, People's Republic of China

Fluorescence carbon dots (CDs) are promising alternatives for the conventional semiconductor quantum dots and organic fluorescence dyes, because CDs possess many interesting properties, including strong fluorescence, high photostability, good biocompatibility, low toxicity, and ease of preparation [20–23]. Several methods for GSH assay based on CDs and MnO_2 have been well-developed. For instance, Wang et al. developed a turn-on fluorescence nanoprobe based on CDs for GSH imaging in living cells [24]. In their work, the fluorescence of CDs is first quenched by MnO_2 and then recovers after GSH-induced MnO_2 decomposition. Lin et al. reported a CD-based probe for the determination of GSH in whole blood samples with similar strategy [25]. Benefiting from the production of Mn^{2+} and fluorescence, Yin et al. designed a magnetic/fluorometric bimodal nanoprobe based on CDs and MnO_2 for the assay of GSH [26]. These previous studies suggest that GSH measurement can be improved by combining CDs and MnO_2. However, in these reported examples, CDs only have a single emission peak. GSH-induced fluctuation in fluorescence intensity can be affected by many factors such as excitation source, variation of probe concentration, and complex environmental conditions [27–29]. A real ratiometric nanoprobe based on intrinsic dual-emission CDs (de-CDs) is still not reported. Hence, it is desirable to explore CDs with intrinsic GSH-sensitive ratiometric fluorescence emission and further construct de-CD-based ratiometric fluorescence probes for GSH measurement in living cells.

In this work, a novel ratiometric fluorescence assay was established for intracellular GSH imaging by combining synthesized dual-emission carbon dots (de-CDs) and MnO_2 nanosheets (MnO_2 NS). As shown in Scheme 1, the de-CDs with dual emission at 435 nm and 516 nm were successfully prepared by one-pot hydrothermal method. Interestingly, de-CDs display intrinsic ratiometric fluorescence emission (F_{435}/F_{516}) against GSH variation. To the best of our knowledge, this is the first example of de-CDs with intrinsic GSH-sensitive ratiometric fluorescence emission. To further fabricate the GSH assay platform, de-CDs were mixed with MnO_2 NS. Due to the adsorption effect of MnO_2 NS, de-CDs can be adsorbed onto the surface of MnO_2 NS and the fluorescence would be quenched. The emission ratio of F_{435}/F_{516} is significantly decreased due to the unique optical property of MnO_2 NS, which exhibits higher absorbance at 435 nm than 516 nm. In the initial state, the emission of de-CDs at 435 nm is suppressed more than that at 516 nm, which results in low ratio of F_{435}/F_{516}. Upon the introduction of GSH, MnO_2 NS is reduced to Mn^{2+} by micromolar GSH, leading to the increase in emission of de-CDs at 435 nm by a larger margin. This makes the ratio F_{435}/F_{516} decrease. The MnO_2 NS is largely decomposed in the presence of 500 μM GSH, which means the ratio F_{435}/F_{516} will not decrease further if de-CDs cannot respond to millimolar GSH. Due to the intrinsic responsiveness of de-CDs, the emission at 516 nm decreases after the GSH concentration increases to millimolar level, while

MnO_2 NS is decomposed completely. Hence, the ratio of F_{435}/F_{516} remains rising with the GSH concentrations from micromolar to millimolar. This novel ratiometric fluorescence GSH nanoprobe can effectively avoid the interference of background noise and auto-fluorescence from cells, thus providing a reliable method for GSH assay.

Experimental

Chemicals and materials

Hydrogen peroxide (30%, wt%), urea, KCl, NaCl, $CaCl_2$, and $MgCl_2$ were purchased from Sinopharm Chemical Reagent Co., Ltd. (China, https://www.sinoreagent.com). GSH (reduced form) and glucose were purchased from Sigma-Aldrich (https://www.sigmaaldrich.com). Other chemicals were analytical reagent grade and purchased from Aladdin Industrial Co., Ltd. (https://www.aladdin-e.com). All chemical reagents were commercially available and used without any further purification. Fetal bovine serum (FBS) and Dulbecco's modified Eagle's medium (DMEM) were purchased from Thermo Fisher Scientific Co., Ltd. (https://www.thermofisher.com). The gibco used in cells was from Zhejiang Tianhang Biotechnology Co., Ltd. (http://www.hzsjq.com). Phosphate buffer saline (PBS) was purchased from Beyotime Biotechnology Co., Ltd. (Shanghai, China, https://www.beyotime.com). A549, Hela, and HepG2 cell lines were provided by the XiangYa School of Medicine, CSU (China, http://xysm.csu.edu.cn).

Instruments

UV-Vis absorption spectra and fluorescence spectra were measured by a UV-Vis spectrophotometer (UV-2100, Shimadzu, Japan) and fluorescence spectrophotometer (F-4600, Shimadzu, Japan), respectively. Transmission electron microscopy (JEM-2100F, JEOL, Japan) and atomic force microscopy (Bioscope, USA) were used to observe the morphology features of synthesized nanomaterial. The cells were incubated in CO_2 incubators (Thermo Scientific, USA). Intracellular GSH images were recorded by Operetta High-Content Imaging System (Eppendorf, Germany).

Screening of de-CDs

To screen the desired de-CDs, many hydrothermal reactions of different precursors were designed. In a typical procedure, about 0.1 g of different precursors was dissolved in 10 mL of ultrapure water and pH was adjusted to help solubilization if necessary. The solution was transferred into Teflon-lined stainless-steel autoclave and heated to 200 °C for 12 h. If fluorescence spectrum of the resultant solution showed dual-emission peaks, centrifugation at 14,000 rpm and dialysis
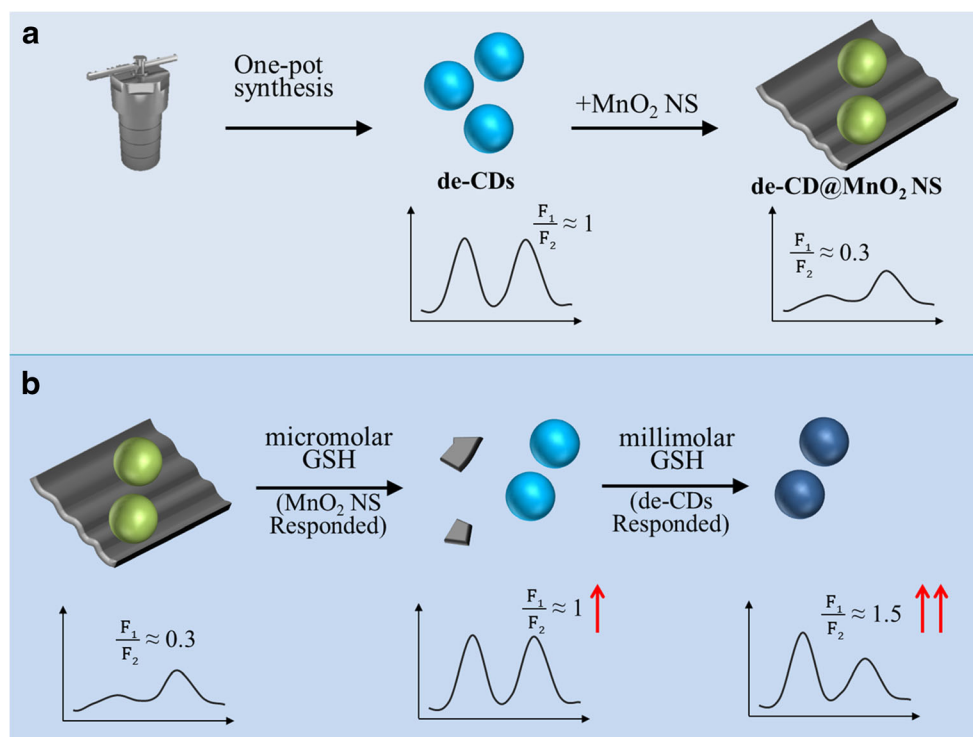
Scheme 1 Synthesis method and GSH detection mechanism of de-CD@MnO$_2$ NS ratiometric nanoprobe. **a** The de-CDs have intrinsic response to millimolar GSH synthesized by one-step hydrothermal treatment, and de-CD@MnO$_2$ nanoprobe is obtained by combination of de-CDs and MnO$_2$ NS. In the process, the dual fluorescence emissions of de-CDs are quenched by MnO$_2$ NS to different degrees. **b** Without GSH, MnO$_2$ NS can quench the fluorescence at 435 nm more powerfully than the fluorescence at 516 nm, which causes a low ratio F_{435}/F_{516}. After decomposition of MnO$_2$ NS by micromolar GSH, fluorescence at 435 nm recovers by a larger margin and the ratio F_{435}/F_{516} increases greatly. If GSH concentration rises to millimolar level, the de-CDs will respond to millimolar GSH and fluorescence at 516 nm will decrease. The intrinsic response of de-CDs to millimolar GSH can cause the ratio F_{435}/F_{516} to increase further

against ultrapure water were performed in order. Fluorescence spectrum of the solution was measured again in order to ensure that both emission peaks were from the synthesized de-CDs.

Preparation of de-CDs

The de-CDs were prepared using calcon-carboxylic acid as precursor and sodium hydroxide as acidity regulator. Briefly, 0.1 g of calcon-carboxylic acid and 0.1 g of sodium hydroxide were dissolved in 10 mL of ultrapure water. The mixture was transferred into a 50-mL Teflon-lined stainless-steel autoclave and heated to 200 °C for 12 h. After cooling to room temperature, the mixture was adjusted to neutral pH with 1 M HCl solution and centrifuged at 14,000 rpm for 20 min twice to remove large particles. The resultant yellow solution was dialyzed in a 3.5 k-MWCO dialysis membrane against ultrapure water for 48 h to remove the small molecular weight impurity. The product was freeze-dried and stored at 4 °C for further use.

Preparation of MnO$_2$ NS

MnO$_2$ NS sample was prepared via free template method according to previous works with minor modifications [30].

Typically, 3 mL of hydrogen peroxide (30%, wt%) and 16 mL of tetramethylammonium hydroxide (10%, v/v) were mixed with 20 mL of ultrapure water. The mixture was quickly transferred into a flask containing 14 mL of manganese chloride solution (0.3 M) on a magnetic stirrer and a dark suspension was observed soon. The reaction was kept stirring overnight to ensure complete oxidation. The resultant suspension was centrifuged at 2000 rpm for 20 min and further washed with methanol and ultrapure water. Solid manganese dioxide was obtained by freeze-drying and re-dispersed in ultrapure water to obtain 0.5 mg/mL manganese dioxide suspension. To prepare the MnO$_2$ NS, the suspension was treated for 1 h with a Sonifier with an output power of 400 W and further ultrasonicated for 10 h. The large particles from mixture were precipitated and removed by centrifugation at 2000 rpm for 30 min and the resultant MnO$_2$ NS was stored at 4 °C for further use.

Optimization of de-CD@MnO$_2$ NS ratiometric nanoprobe

Different volumes of 29.4 μg mL^{-1} solution of MnO$_2$ NS were mixed with 10 μL of 0.3 mg mL^{-1} de-CDs in tubes. Then, phosphate buffer (20 mM, pH 7.4) was added into the

tubes to obtain de-CD@MnO$_2$ NS ratiometric nanoprobe containing specific concentrations of MnO$_2$ NS. Fluorescence spectra of the solution excited at 365 nm were measured at least 30 min after mixing adequately.

Fluorescence stability test

To investigate the fluorescence stability in physiological conditions, different interfering substances (final concentration of GSH was 10 mM; final concentrations of histidine and aspartic acid were 250 μM, cysteine and ascorbic acid were 100 μM, and others were 1 mM) were added into the nanoprobe, respectively. Before measuring fluorescence spectra, the resultant mixtures were incubated under gentle shaking at 37 °C for 1 h.

Determination of GSH

Different volumes of GSH and phosphate buffer (20 mM, pH 7.4) were added into tubes containing 70 μL of MnO$_2$ NS and 10 μL of de-CDs. Fluorescence spectra of the solution excited at 365 nm were measured after at least 10 min of adequate mixing.

Cell culture and cytotoxicity assay

All cells were cultured in DMEM media (high glucose) with 10% (v/v) fetal bovine serum, 100 U mL^{-1} penicillin and 100 μg mL^{-1} streptomycin at 37 °C and 5% CO$_2$ atmosphere.

Cell viability was determined by cytotoxicity assay using CCK-8 method. Briefly, 100 μL of cell suspension was planted in 96-well plates (8000 cells per well) and incubated for 24 h. Different concentrations of de-CDs were added to each well and subsequently cultured for 24 h. Before adding 10 μL of CCK-8 reagent, each well was gently washed three times with PBS. After about half an hour, absorbance of each well at 450 nm was measured. The same procedure was followed for the subsequent cytotoxicity assay of de-CD@MnO$_2$ NS ratiometric nanoprobe.

Ratiometric imaging of glutathione in living cells

A549 cells were planted in 96-well plates (8000 cells per well) and incubated for 24 h. After removing the DMEM media, the cells were washed with PBS (pH 7.4) three times and then cultured with DMEM media. To increase or decrease the concentrations of GSH in A549 cells, the cells were treated respectively with α-lipoic acid (LPA, 500 μM) or buthionine sulfoximine (BSO, 100 μM) for 24 h and 6 h. All groups were washed with PBS three times, including the group with LPA, the group with BSO, and the control group (untreated with LPA and BSO). They were subsequently co-incubated with 20 μg mL^{-1} de-CD@MnO$_2$ NS ratiometric nanoprobe for 3 h.

The blank group was cultured with DMEM without addition of LPA, BSO, and nanoprobe. The cells were then washed with PBS three times and analyzed using high-content imaging system (excitation: 355–385 nm, blue channel: 430–500 nm, green channel: 500–550 nm).

Results and discussions

Preparation and characterization of de-CDs

As a novel fluorescence nanomaterial, carbon dots are superior to other classical fluorescence materials in many aspects, especially in terms of their biological compatibility and fluorescence tunability [31]. By introducing different surface states during the synthesis process, such as hydrothermal treatment, carbon dots can be simply translated into de-CDs which exhibit dual emissions under single-wavelength excitation [32, 33]. As listed in Table S1, different precursors were hydrothermally treated to form carbon cores and prepare carbon dots. Most of the resultant carbon dots exhibited single emission and their best emission wavelength was in the range of 400–450 nm, which was likely due to conjugated carbon skeletons [34]. After a round of screening through hydrothermal treatment with different precursors, de-CDs synthesized by one-step hydrothermal treatment with calcon-carboxylic acid were selected as the potential dual-emission fluorescence agent and further investigated.

Optical properties of the synthesized de-CDs were first explored. Figure 1a depicts the absorption and fluorescence properties in ultraviolet-visible region. The de-CDs exhibited a broad absorption band under 400 nm and two shoulders at 280 nm and 330 nm, respectively. The broad absorption was possibly caused by different sizes of de-CDs and the shoulders are probably due to the π–π* transition of aromatic carbons in the cores of de-CDs. Two emission peaks at 435 nm and 516 nm were observed in the fluorescence spectra, which preliminarily confirmed the formation of de-CDs during hydrothermal treatment. Consistent with the absorption and fluorescence properties, the solution of de-CDs appeared light yellow when illuminated by white light due to obvious absorption under 400 nm. When excited at 365 nm, it appeared bright cyan, which was likely caused by overlapping of two fluorescence peaks. As shown in Fig. 1b, the detailed fluorescence emission properties under excitations from 350 to 410 nm were measured. The intensity of both emission peaks gradually reduced with the increase in excitation wavelength, and the emission peak at 435 nm declined more sharply. The dual-emission peaks reached similar intensity under excitation at 365 nm. In order to obtain enough room for increasing or decreasing the wavelength in follow-up work, 365 nm was selected as the best excitation wavelength. Fourier-transform infrared (FT-IR) spectroscopy was used to study the surface
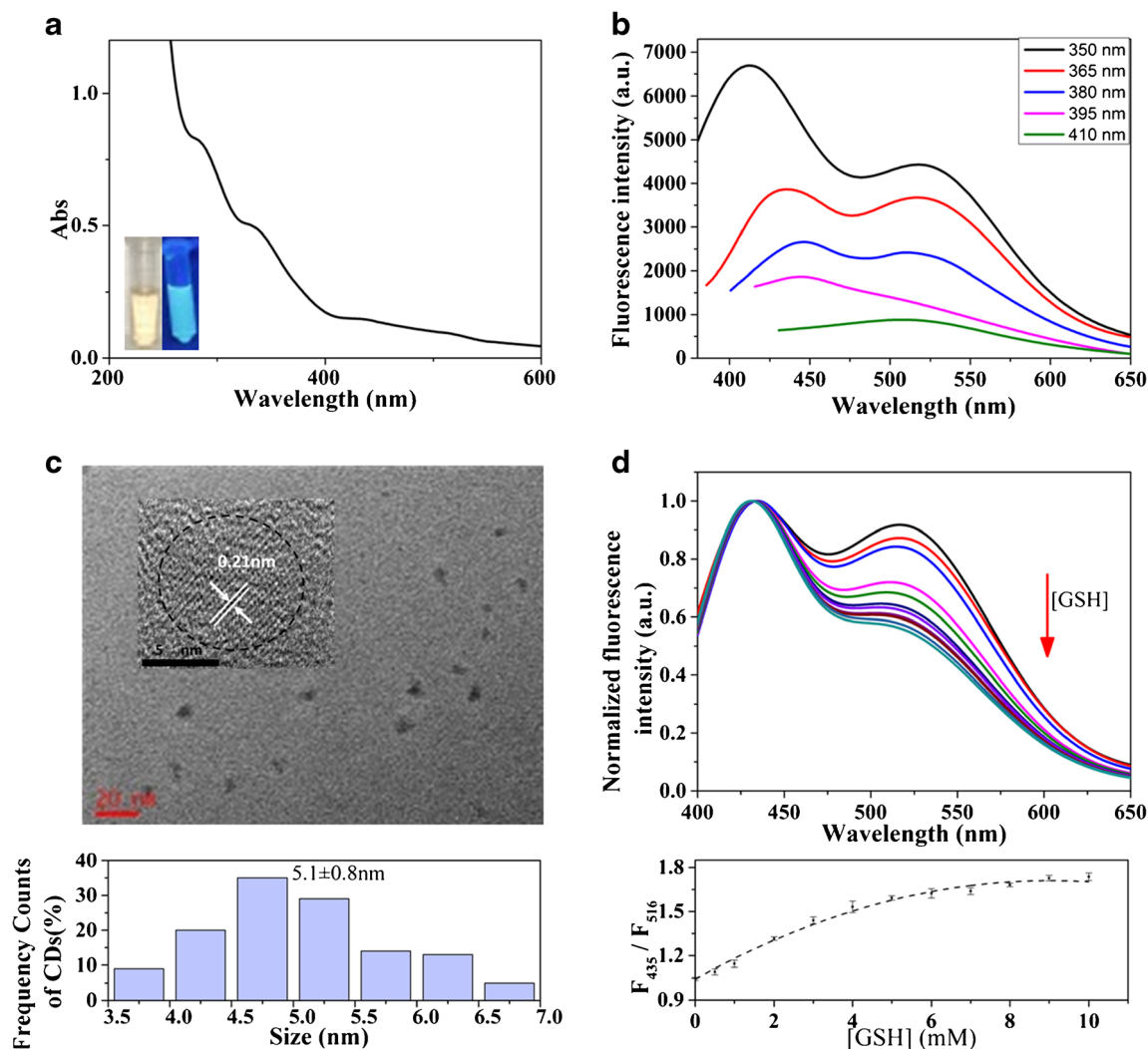
Fig. 1 The optical properties and morphology features of de-CDs. **a** The UV-Vis absorption spectrum of de-CDs, inset shows the photos of de-CDs solution irradiated by white light (left) and UV light (right) at 365 nm. **b** Fluorescence spectra of de-CDs with excitation at different wavelengths. **c** TEM image of de-CDs, the column chart below TEM image is the particle size distribution of de-CDs (125 particles included). **d** Fluorescence spectra of de-CDs with different concentrations of GSH after normalizing, the concentrations of GSH are 0, 0.5, 1, 2, … 9, and 10 mM from top to bottom. The diagram below is the relationship between fluorescence ratio F_{435}/F_{516} and GSH concentration

functional groups of de-CDs (Fig. S1). Some characteristic functional groups were observed, such as N–H (3440 cm^{-1}), C=N (1638 cm^{-1}), C=C (1559 and 1454 cm^{-1}), O–H (1190 cm^{-1}), and C–O (1053 cm^{-1}). This indicated that de-CDs contain aromatic structures, and the dual-emission property may be caused by different aromatic structures or surface states.

Then, the morphology features of synthesized de-CDs were characterized by transmission electron microscopy (TEM) and atomic force microscopy (AFM). As shown in Fig. 1c, the de-CDs were mostly oval shape. The TEM images also indicated high degree of crystallinity and the spacing of 0.21 nm corresponded to the (100) in-plane lattice of graphene. After counting the diameters of 125 de-CDs by ImageJ software, the particle sizes were determined to be in the range of 3.5 to 7 nm

and the calculated result of average diameter was 5.1 nm. The AFM results showed that the topographic heights of de-CDs were about 5.5 nm, which is consistent with TEM. This result further indicated that the synthesized de-CDs were nearly spherical (Fig. S2). Thus, the synthesis of de-CDs was strongly confirmed.

The GSH-response property of de-CDs was tested next. As shown in Fig. 1d, the millimolar GSH can reduce fluorescence intensity of de-CDs at 516 nm specifically, resulting in an obvious increase in F_{435}/F_{516}. The ratio F_{435}/F_{516} remained constant after sustained illumination because of the similar degree of decline in both fluorescence peaks. This ensured more reliable measurement results (Fig. S3). However, the signal-to-background ratio of de-CDs against GSH was slightly low. To expand the application of de-CDs, a GSH

nanoprobe with higher sensitivity was further constructed by employing the advantages of MnO_2 NS. As previously reported, MnO_2 NS have a broad UV-Vis absorption spectrum from 250 to 600 nm and can respond to GSH with high sensitivity and selectivity [24, 25, 35].

Feasibility study and optimization of detection strategy

Before feasibility study, MnO_2 NS was prepared and characterized (Fig. S4). The synthesized MnO_2 NS exhibited a strong absorption band in ultraviolet and visible region. Notably, it was found that absorbance of MnO_2 NS was highly related to wavelength. For example, the absorbance declined significantly after 400 nm. TEM images indicate that MnO_2 NS was less than 150 nm and with a thin thickness, which can facilitate the entry of a MnO_2 NS–based nanoprobe into living cells. After the key characterizations, the synthesized MnO_2 NS was confirmed to be consistent with previous reports and suitable for subsequent physiological applications [30].

To study the feasibility of detection strategy, it is critical to confirm the difference in fluorescence suppression between the two fluorescence peaks of de-CDs and subsequent ratio recovery. As shown in Fig. 2a, the absorbance of MnO_2 NS at 435 nm was much higher than its absorbance at 516 nm. This difference significantly improved the quenching effect between MnO_2 NS and the fluorescence of de-CDs at 435 nm (dotted black line). In the comparison of fluorescence of de-

CDs with or without adding MnO_2 NS (blue line and red solid line in Fig. 2a, respectively), the difference in suppression efficiency between the two fluorescence peaks was observed more clearly. As expected, GSH can decompose MnO_2 NS and recover the ratio of the two fluorescence peaks. This result indicates that the proposed strategy is basically feasible (shown as red solid line and dotted red line in Fig. 2a). However, it should be pointed out that 500 μM of GSH decomposed most of the MnO_2 NS and restored the fluorescence spectrum back to its original state without MnO_2 NS. In other words, higher concentrations of GSH would not trigger fluorescence response if de-CDs have no intrinsic response to millimolar GSH. Hence, the intrinsic response of de-CDs to millimolar GSH is the vital factor when applied to physiological conditions. The quenching time between MnO_2 NS and de-CDs was investigated via monitoring the change in fluorescence intensity before and after adding MnO_2 NS. As shown in Fig. S5a, after adding MnO_2 NS, the fluorescence signal dropped almost immediately, and then showed a little disturbance, which was probably caused by adsorption and mixing processes. Fluorescence signal reached a balance eventually 10 min after adding MnO_2 NS. The result indicates that the subsequent experiments should be performed at least 10 min after mixing de-CDs and MnO_2 NS.

Subsequently, the fluorescence quenching properties of different concentrations of MnO_2 NS were investigated. As shown in Fig. 2b, the fluorescence of de-CDs decreased gradually upon increasing the concentration of MnO_2 NS in
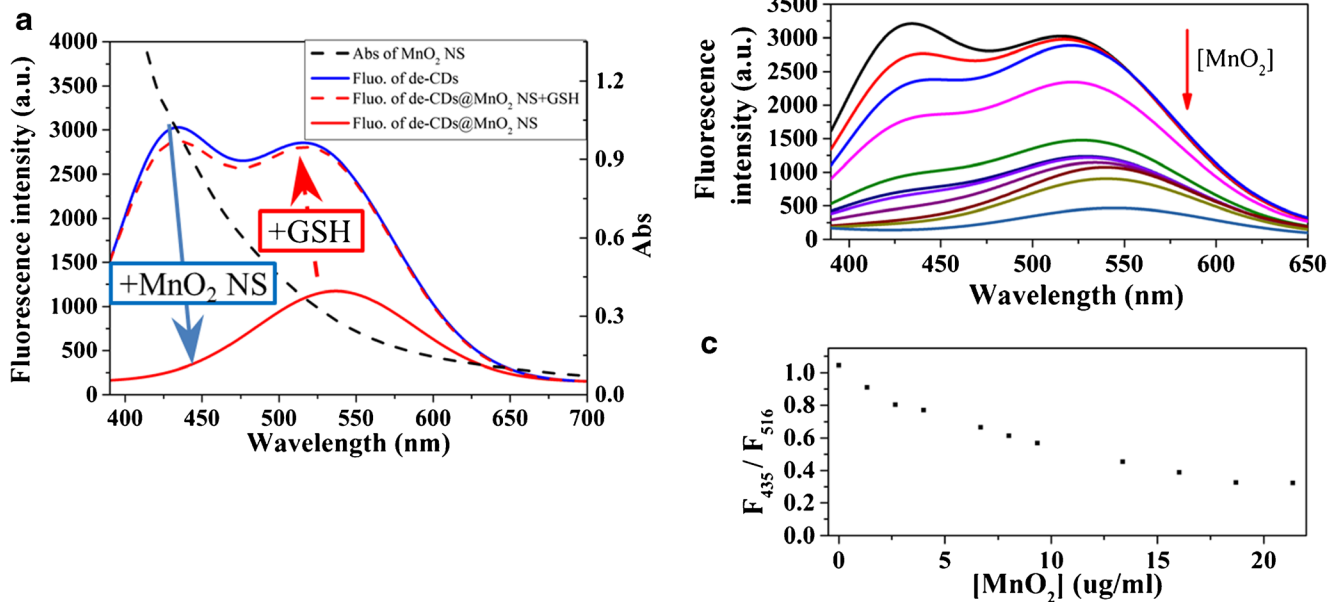

Fig. 2 Feasibility study and optimization of detection strategy. **a** Fluorescence of de-CDs (blue line), de-CD@MnO_2 NS ratiometric nanoprobe (red line), and de-CD@MnO_2 NS ratiometric nanoprobe incubated with 500 μM GSH (dotted red line), dotted black line is absorption of MnO_2 NS. **b** Fluorescence spectra of de-CDs incubated with different concentrations of MnO_2 NS (from top to bottom: 0, 1.3, 2.7, 4.0, 6.7, 8.0, 9.4, 13.4, 16.0, 18.7, 21.4 μg mL^{-1}, respectively). **c** Corresponding fluorescence ratio of de-CDs in the presence of different concentrations of MnO_2 NS

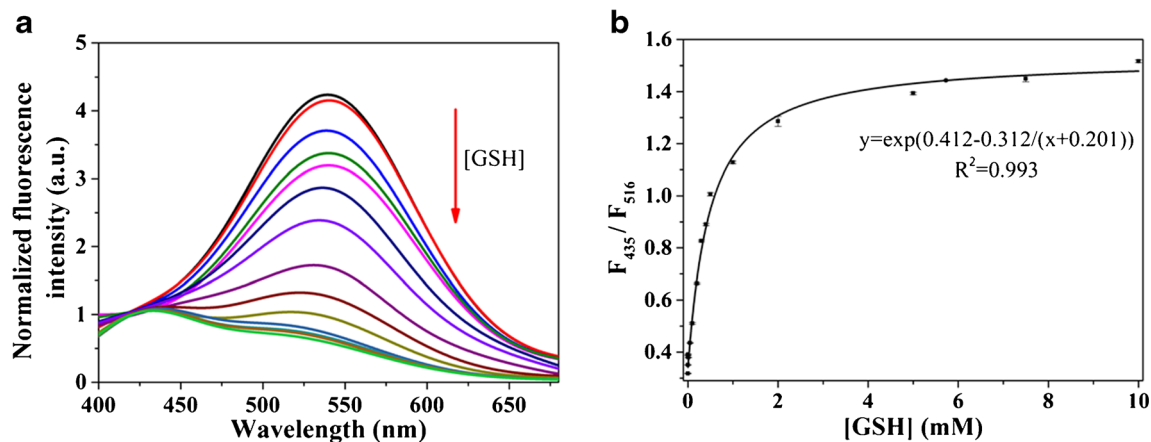**Fig. 3** GSH-response performance of de-CD@MnO$_2$ NS ratiometric nanoprobe. **a** Fluorescence of de-CD@MnO$_2$ NS ratiometric nanoprobe with different concentrations of GSH after normalizing (from top to bottom: 0, 1, 5, 10, 50, 100, 200, 400, 500, 1000, 2000, 5000, 7500, 10,000 μM, respectively). **b** Relationship between fluorescence ratio F_{435}/F_{516} of de-CD@MnO$_2$ NS ratiometric nanoprobe and the GSH concentration

solution. It can also be clearly observed that the absorbance of MnO$_2$ NS at 435 nm was much higher than that at 516 nm. This difference significantly improved the quenching effect between MnO$_2$ NS and the fluorescence of de-CDs at 435 nm, thus resulting in a low ratio of F_{435}/F_{516}. The ratio of F_{435}/F_{516} decreased to 0.32 after incubation with 18.7 μg mL^{-1} MnO$_2$ NS and then reached a plateau. Therefore, 18.7 μg mL^{-1} MnO$_2$ NS was selected to construct the nanoprobe in this study. After fitting the fluorescence data to the Stern-Volmer equation and modified Stern-Volmer equation, it was found that these equations deviated from the data (Supporting Information). This may indicate that there were some other effects involved in the quenching process, such as inner filter effect (IFE) [36]. Some similar nanocomposites based on MnO$_2$ and nano-sized fluorescence materials have been developed, such as MnO$_2$-carbon dots and MnO$_2$-upconversion nanoparticles. For these materials, the quenching processes are mainly ascribed to IFE and fluorescence resonance energy transfer (FRET) [25, 37–39]. Thus, it was considered that the observed quenching process resulted from IFE and FRET.

Investigation of GSH ratiometric response performance

The GSH ratiometric response performance of de-CD@MnO$_2$ NS was studied. First, the interaction time between de-CD@MnO$_2$ NS ratiometric nanoprobe and GSH was investigated via monitoring the change of fluorescence intensity before and after addition of GSH. As shown in Fig. S5b, after adding GSH, fluorescence signal increased almost immediately and then reached a balance within less than 3 min. This indicates that the fluorescence recovery was a quick process. To allow sufficient time for the decomposition, the follow-up

study was conducted 30 min after adequate mixing of de-CDs and MnO$_2$ NS.

Different concentrations of GSH were then added into de-CD@MnO$_2$ NS ratiometric nanoprobe in buffer. As shown in Fig. S6a, the two emission peaks recovered ratiometrically after decomposition of MnO$_2$ NS by micromolar GSH. The higher concentrations of GSH subsequently reduced the fluorescence intensity of the ratiometric nanoprobe at 516 nm (Fig. S6b). After normalization, the fluorescence ratio F_{435}/F_{516} gradually increased with the increase in GSH within micromole to millimole range (Fig. 3a). Exponential curve fitting was applied to describe the data. The fitted curve with correlation coefficient (R^2) of 0.993 can be utilized to quantify the concentrations of GSH (Fig. 3b). The detection limit reached 0.6 μM based on the 3σ rule.
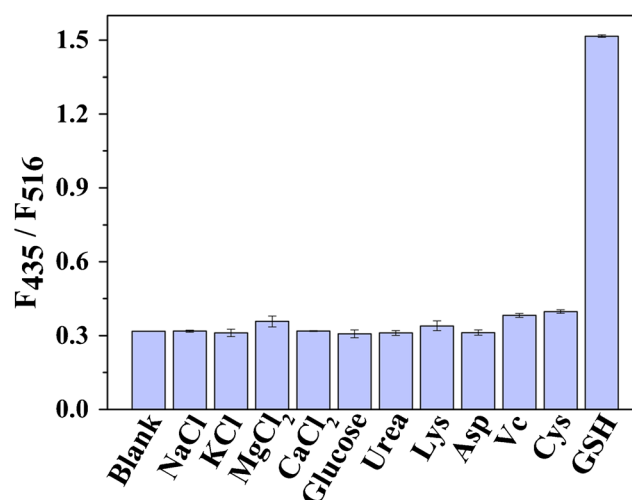

Fig. 4 Fluorescence ratio of de-CD@MnO$_2$ NS ratiometric nanoprobe in the presence of GSH or different interfering substances (final concentrations: GSH was 10 mM, histidine and aspartic acid were 250 μM, cysteine and ascorbic acid were 100 μM, and others were 1 mM)
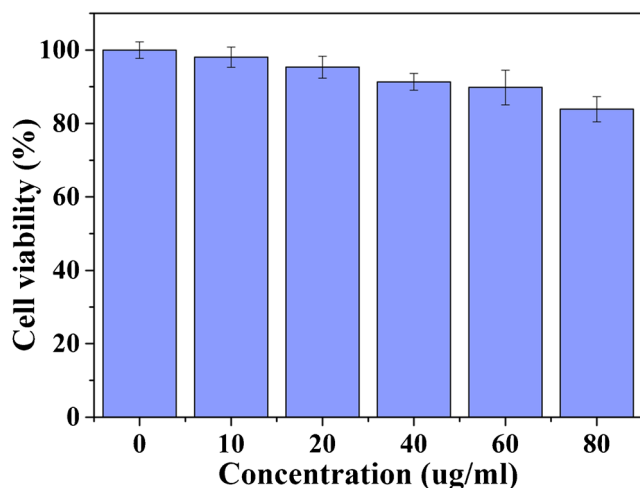
Fig. 5 Cell viability of A549 cells after incubation with different concentrations of de-CD@MnO$_2$ NS ratiometric nanoprobe

The selectivity of nanoprobe was estimated by parallel measurement of the ratiometric response of de-CD@MnO$_2$ NS to many common species in the human body, including ions, sugars, amino acids, metabolites, and reducing substances. The addition amounts were according to the concentrations of these species in living cells or slightly higher concentrations [24, 26]. As shown in Fig. 4, the influence of these investigated

interferents on the assay performance of the proposed nanoprobe toward GSH was negligible. The fluorescence stability of de-CD@MnO$_2$ NS in different pH (from 5 to 8) was investigated as well. It was found that the fluorescence changes caused by pH were less than 10% (data are not shown). Taken together, these results substantiate the intracellular potential application of de-CD@MnO$_2$ NS. To check the reversibility of the nanoprobe, GSH and hydrogen peroxide were added into de-CD@MnO$_2$ NS in order, and fluorescence of the sample was measured continuously. After adding hydrogen peroxide, the fluorescence did not decrease again. The result suggests the irreversibility of the nanoprobe. This may be because the MnO$_2$ NS cannot regenerate after it is decomposed by GSH.

Biocompatibility test

Apart from selectivity, biocompatibility is another critical factor to be taken into account in the design of an intracellular assay platform. Hence, CCK-8 assays were performed to further evaluate the biocompatibility. As shown in Fig. 5, no obvious cytotoxicity was observed after incubation with nanoprobe at concentrations below 60 μg mL^{-1}. Moreover, about 90% cells still maintained their cell viability after 60 μg mL^{-1} nanoprobe treatment. These results indicate that

Fig. 6 Intracellular GSH imaging using de-CD@MnO$_2$ NS ratiometric nanoprobe. No treatments were performed for the blank group and other groups were labeled by de-CD@MnO$_2$ NS ratiometric nanoprobe. Before labeling, LPA group and BSO group were pretreated with LPA (0.5 mM) and BSO (0.1 mM) for 24 h and 1 h, respectively. Excitation: 355–385 nm, blue channel: 430–500 nm, green channel: 500–550 nm. Scale bars = 20 μM
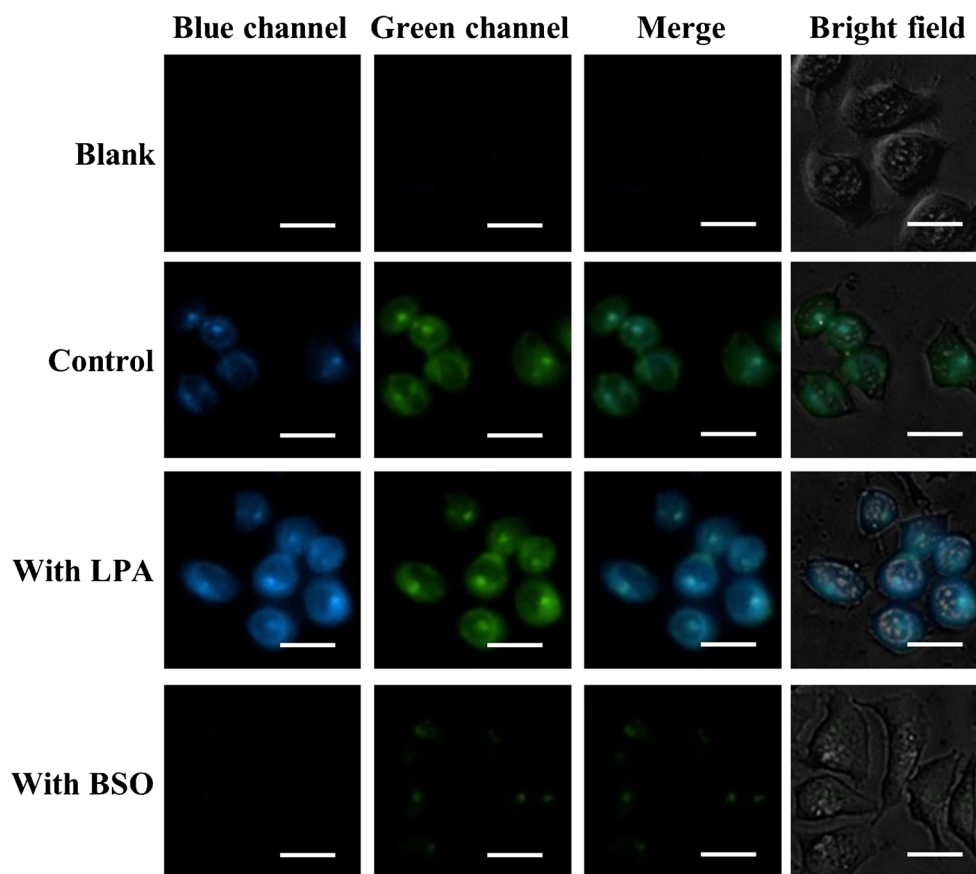
the de-CD@MnO$_2$ NS ratiometric nanoprobe at normal dosages has good biocompatibility and the potential for intracellular GSH imaging.

Ratiometric intracellular GSH imaging

Next, the ability of the proposed nanoprobe to reflect the intracellular GSH level was investigated (Fig. 6). After incubation with the nanoprobe, A549 cells displayed blue emission and slightly stronger green emission under UV light excitation. This is probably due to the decomposition of some MnO$_2$ NS by intrinsic intracellular GSH. In comparison, after depletion of intracellular GSH by treatment with buthionine sulfoximine (BSO, synthesis inhibitor of GSH), only negligible fluorescence emission was observed. This indicates that low intracellular GSH level cannot decompose MnO$_2$ NS and the fluorescence suppression existed in living cells. The capability of higher GSH-level detection was studied through improving intracellular GSH level by α-lipoic acid (LPA, synthesis accelerator of GSH) pretreatment. Both blue emission and green emission were enhanced. This was probably due to the more thorough decomposition of MnO$_2$ NS and failure of fluorescence suppression. It is necessary to point out that two superimposed images with and without LPA pretreatment showed another difference apart from fluorescence intensity. The merged image with LPA pretreatment preferred blue. The result indicates that high intracellular concentration of GSH decreased the green fluorescence due to the intrinsic response of de-CDs to millimolar GSH. The intracellular GSH imaging results are highly consistent with extracellular measures. All the results demonstrate that the ratiometric nanoprobe can detect the GSH level over a wide concentration range with high selectivity and universality.

GSH is the essential substance in all living cells. To investigate whether this nanoprobe can be applied for intracellular assay of GSH in other cells, HepG2 cells and Hela cells were treated with the de-CD@MnO$_2$ NS nanoprobe. As shown in Fig. S7, strong blue fluorescence emission was observed in HepG2 cells compared with green fluorescence, while the opposite effect was observed in Hela cells. These results are consistent with the intracellular GSH level reported by Liu et al. [37]. Thus, these results demonstrate that the de-CD@MnO$_2$ NS nanoprobe is a viable and reliable tool for ratiometric fluorescence imaging of GSH in living cells. However, due to the relatively high detection limit compared with some recent works, the de-CD@MnO$_2$ NS nanoprobe is not suitable for biological fluids like blood and urine. Furthermore, the irreversibility of the de-CD@MnO$_2$ NS nanoprobe limits its applications, such as continuous GSH monitoring. Related efforts will be made in our lab to address these limitations in future work.

Conclusion

In conclusion, a new ratiometric fluorescence nanoprobe was developed for GSH assay by combination of de-CDs and MnO$_2$ NS. The nanoprobe takes advantage of the unique dual-emission property of de-CDs and the properties of MnO$_2$ NS, including the excellent fluorescence quenching efficiency and response behavior toward GSH. Therefore, the assay not only exhibited reliable responses toward GSH function in aqueous solution but also enabled ratiometric monitoring of the dynamic variation of GSH in living cells. The ratiometric mode makes the nanoprobe more resistant to interference and suitable for quantification in complex biological environment. Thus, the new ratiometric nanoprobe is expected to be widely used in biological assays and biomedical field, and shows great potential for ratiometric measurements and quantifications in biological samples. However, the detection limit needs to be further reduced, and the detection irreversibility must be solved. These aspects will be addressed in our future work.

Compliance with ethical standards

Conflict of interest The authors declare that they have no competing interests.

References

1. Ren X, Zou L, Zhang X, Branco V, Wang J, Carvalho C, Holmgren A, Lu J (2017) Redox signaling mediated by thioredoxin and glutathione systems in the central nervous system. Antioxid Redox Sign 27:13

2. Calabrese G, Morgan B, Riemer J (2017) Mitochondrial glutathione: regulation and functions. Antioxid. Redox Sign 27:15

3. Sedlak TW, Paul BD, Parker GM, Hester LD, Snowman AM, Taniguchi Y, Kamiya A, Snyder SH, Sawa A (2019) The glutathione cycle shapes synaptic glutamate activity. P Natl Acad Sci U S A 116:2701–2706

4. Benhar M, Shytaj IL, Stamler JS, Savarino A (2016) Dual targeting of the thioredoxin and glutathione systems in cancer and HIV. J Clin Invest 126:1630–1639

5. Géhla Z, Bakondi E, Resch MD, Hegedűs C, Kovács K, Lakatos P, Szabó A, Nagy Z, Virág L (2016) Diabetes-induced oxidative stress in the vitreous humor. Redox Biol 9:100–103

6. Gorrini C, Mak TW (2019) Glutathione metabolism: an Achilles' heel of ARID1A-deficient tumors. Cancer Cell 35:161–163

7. Peng HP, Jian ML, Huang ZN, Wang WJ, Deng HH, Wu WH, Liu AL, Xia XH, Chen W (2018) Facile electrochemiluminescence sensing platform based on high-quantum-yield gold nanocluster probe for ultrasensitive glutathione detection. Biosens Bioelectron 105:71–76

8. Shi W, Song B, Shi W, Qin X, Liu Z, Tan M, Wang L, Song F, Yuan J (2018) Bimodal phosphorescence–magnetic resonance imaging nanoprobes for glutathione based on MnO2 nanosheet–Ru(II) complex nanoarchitecture. ACS Appl Mater Interfaces 10: 27681–27691

9. Zhang Y, Zhang W, Chen K, Yang Q, Hu N, Suo Y, Wang J (2018) Highly sensitive and selective colorimetric detection of glutathione via enhanced Fenton-like reaction of magnetic metal organic framework. Sensor Actuat B – Chem 262:95–101

10. Hu X, Liu X, Zhang X, Cao H, Huang Y (2019) MnO2 nanowires tuning of photoluminescence of alloy Cu/Ag NCs and thiamine enables a ratiometric fluorescent sensing of glutathione. Sensor Actuat B – Chem 286:476–482

11. Tang M, Zhu B, Wang Y, Wu H, Chai F, Qu F, Su Z (2019) Nitrogen- and sulfur-doped carbon dots as peroxidase mimetics: colorimetric determination of hydrogen peroxide and glutathione, and fluorimetric determination of lead(II). Microchim Acta 186:604

12. Tang X, Zeng X, Liu H, Yang Y, Zhou H, Cai H (2019) A nanohybrid composed of MoS2 quantum dots and MnO2 nanosheets with dual-emission and peroxidase mimicking properties for use in ratiometric fluorometric detection and cellular imaging of glutathione. Microchim Acta 186:572

13. Wu P, Hou X, Xu JJ, Chen HY (2016) Ratiometric fluorescence electrochemiluminescence and photoelectrochemical chemo/biosensing based on semiconductor quantum dots. Nanoscale 8: 8427–8442

14. Huang X, Song J, Yung BC, Huang X, Xiong Y, Chen X (2018) Ratiometric optical nanoprobes enable accurate molecular detection and imaging. Chem Soc Rev 47:2873–2920

15. Gui R, Jin H, Bu X, Fu Y, Wang Z, Liu Q (2019) Recent advances in dual-emission ratiometric fluorescence probes for chemo/biosensing and bioimaging of biomarkers. Coordin Chem Rev 383:82–103

16. Ma Z, Wu T, Li P, Liu M, Huang S, Li H, Zhang Y, Yao S (2019) A dual (colorimetric and fluorometric) detection scheme for glutathione and silver (I) based on the oxidase mimicking activity of MnO2 nanosheets. Microchim Acta 186:498

17. Yin C, Tang Y, Li X, Yang Z, Li J, Li X, Huang W, Fan QA (2018) Single composition architecture-based nanoprobe for ratiometric photoacoustic imaging of glutathione (GSH) in living mice. Small 14:1703400

18. Qi S, Liu W, Zhang P, Wu J, Zhang H, Ren H, Ge J, Wang P (2018) A colorimetric and probe for highly selective detection of glutathione in the mitochondria of living cells. Sensor Actuat B - Chem 270:459–465

19. Zheng J, Wu Y, Xing D, Zhang T (2019) Synchronous detection of glutathione/hydrogen peroxide for monitoring redox status in vivo with a ratiometric upconverting nanoprobe. Nano Res 12:931–938

20. Zhi B, Cui Y, Wang S, Frank BP, Williams DN, Brown RP, Melby ES, Hamers RJ, Rosenzweig Z, Fairbrother DH, Orr G, Haynes CL (2018) Malic acid carbon dots: from super-resolution live-cell imaging to highly efficient separation. ACS Nano 12:5741–5752

21. Hassan M, Gomes VG, Dehghani A, Ardekani SM (2018) Engineering carbon quantum dots for photomediated theranostics. Nano Res 11:1–41

22. Du J, Xu N, Fan J, Sun W, Peng X (2019) Carbon dots for in vivo bioimaging and theranostics. Small 15:1805087

23. Yan F, Sun Z, Zhang H, Sun X, Jiang Y, Bai Z (2019) The fluorescence mechanism of carbon dots, and methods for tuning their emission color: a review. Microchim Acta 186:583

24. He D, Yang X, HeX MK, He X, Zou Z (2015) A sensitive turn-on fluorescent probe for intracellular imaging of glutathione using single-layer MnO2 nanosheet-quenched fluorescent carbon quantum dots. Chem Commun 51:14764–14767

25. Wang Y, Jiang K, Zhu J, Zhang L, Lin H (2015) A FRET-based carbon dot–MnO2 nanosheet architecture for glutathione sensing in human whole blood samples. Chem Commun 51:12748–12751

26. Xu Y, Chen X, Chai R, Xing C, Li H, Yin XB (2016) A magnetic/fluorometric bimodal sensor based on a carbon dots–MnO2 platform for glutathione detection. Nanoscale 8:13414–13421

27. Cui Y, Liu R, Ye F, Zhao S (2019) Single-excitation dual-emission biomass quantum dots: preparation and application for ratiometric fluorescence imaging of coenzyme A in living cells. Nanoscale 11: 9270–9275

28. Chen L, Park SJ, Wu D, Kim HM, Yoon J (2019) A two-photon fluorescent probe for colorimetric and ratiometric monitoring of mercury in live cells and tissues. Chem Commun 55:1766–1769

29. Wu S, Min H, Shi W, Cheng P (2019) Multicenter metal–organic framework-based ratiometric fluorescent sensors. Adv Mater 2019: e1805871. https://doi.org/10.1002/adma.201805871

30. Fan H, Zhao Z, Yan G, Zhang X, Yang C, Meng H, Chen Z, Liu H, Tan W (2015) A smart DNAzyme–MnO2 nanosystem for efficient gene silencing. Angew Chem Int Edit 54:4801–4805

31. Zhu Z, Zhai Y, Li Z, Zhu P, Mao S, Zhu C, Du D, Belfiore LA, Tang J, Lin Y (2019) Red carbon dots: optical property regulations and applications. Mater Today 30:52–79

32. Shangguan J, He D, He X, Wang K, Xu F, Liu J, Tang J, Yang X, Huang J (2016) Label-free carbon-dots-based ratiometric fluorescence pH nanoprobes for intracellular pH sensing. Anal Chem 88: 7837–7843

33. Song W, DuanW LY, Ye Z, Chen Y, Chen H, Qi S, Wu J, Liu D, Xiao L, Ren C, Chen X (2017) Ratiometric detection of intracellular lysine and pH with one-pot synthesized dual emissive carbon dots. Anal Chem 89:13626–13633

34. Dong Y, Shao J, Chen C, Li H, Wang R, Chi Y, Lin X, Chen G (2012) Blue luminescent graphene quantum dots and graphene oxide prepared by tuning the carbonization degree of citric acid. Carbon 50:4738–4743

35. Chen J, Meng H, Tian Y, Yang R, Du D, Li Z, Qu L, Lin Y (2019) Recent advances in functionalized MnO2 nanosheets for biosensing and biomedicine applications. Nanoscale Horiz 4:321–338

36. Zhai W, Wang C, Yu P, Wang Y, Mao L (2014) Single-layer MnO2 nanosheets suppressed fluorescence of 7-hydroxycoumarin: mechanistic study and application for sensitive sensing of ascorbic acid in vivo. Anal Chem 86:12206–12213

37. Deng R, Xie X, Vendrell M, Chang YT, Liu X (2011) Intracellular glutathione detection using MnO2-nanosheet-modified upconversion nanoparticles. J Am Chem Soc 133:20168–20171

38. Peng C, Xing H, Fan X, Xue Y, Li J, Wang E (2019) Glutathione regulated inner filter effect of MnO2 nanosheets on boron nitride quantum dots for sensitive assay. Anal Chem 91:5762–5767

39. Cai Q Y, Li J, Ge J, Zhang L, Hu Y L, Li Z H, Qu L B (2015) A rapid fluorescence "switch-on" assay for glutathione detection by using carbon dots–MnO2 nanocomposites. 72: 31-36